

# Modeling Simulations and Instrumentation of High Pressure Roller Crusher for the Silicon Carbide Production

SYLVESTER SEDEM DJOKOTO      HAMID REZA KARIMI

Department of Engineering, Faculty of Engineering and Science,  
University of Adger, N-4898 Grimstad, NORWAY

Emails: sedem.djok@gmail.com; hamid.r.karimi@uia.no

**Abstract:** - This paper describes the modeling, simulation and the instrumentation of High Pressure Roller Crusher (HPRC) for the production of silicon carbide grains. The study is to make a model and then simulate a High Pressure Roller Crusher. Selection of sensors for the HPRC is also important in this study. A High Pressure Roller Crusher (HPRC) is an important part in the production of silicon carbide, where the grains are crushed into powder form and then sieved into specified sizes based on its usage. This paper will present a model based on Johanson's theory for roller compactors, considering all the delays. The non-linearity or delays were handled in matlab using. Conclusions were drawn at end of the paper.

**Key-Words:** - High Pressure Roller Crusher (HPRC), Silicon Carbide, Instrumentation

## 1 Introduction

The discovery of silicon carbide dated back to about 100 years ago, when a struggling scientist, once employed by Thomas Edison, dreamed of becoming wealthy. What is a better way to riches, he reasoned, than by making artificial diamonds?

This young scientist, Dr. Edward Goodrich Acheson, had invented silicon carbide (SiC), the first man-made abrasive and substance hard enough to cut glass.

Saint Gobain Ceramics Norway is one the leading producers of Silicon Carbide. The milling process of silicon carbide happens at different stages. The Arendal branch of this company produces Silicon Carbide grain into different sizes that is turned into slurry to aid the cutting of solar cells.

The modeling and simulation of the roller compactor will be an integral part of the process such that suitable controllers could be designed in the future. This paper considered a two input and two output model design based on Johanson's theory for roller compactors. Due to non linearity a Padé approximation approach was used to linearize the system. The modeling was done using Matlab tools and Simulink to verify the model.

### 1.1 Milling Process

Acheson's discovery of Silicon Carbide became Carborundum, the trademark for silicon carbide and the name given to the company he started. No other company in the world that has more expertise with silicon carbide than Saint-Gobain. They invented it, developed numerous variations of it and make more of it for high-performance components than anyone else in the world. Saint Gobain has companies in Arendal and Lillesand in Norway for the production of Silicon Carbide (SiC)

Today Saint-Gobain has earned a reputation for providing advanced, high-tech ceramic components to worldwide markets. These markets span multiple industries, requiring materials that are resistant to extreme temperature, thermal shock, abrasion and corrosion.

Silicon Carbide (SiC) is a material that is very useful for different purposes. It has properties such as:

- High hardness (only diamond is harder), compressive strength and light weight. Hardness (Knoop): 2800 kg/mm<sup>2</sup> at room temperature
- It exhibits reduced micro porosity resulting in a higher Weibull modulus and increased flexural strength Flexural strength (4 pt.): 55,000 psi (380 MPa) Fracture toughness: 4.20 x 10<sup>3</sup> lb/in<sup>2</sup> x in<sup>1/2</sup>

Modulus of elasticity (RT): 59 x 106 lb/in2 (410 GPa)

- Very good temperature resistance; the thermal conductivity of silicon carbide, combined with its low thermal expansion, produces excellent thermal-shock resistance far better than tungsten carbide, aluminum oxide and RB silicon nitride. These properties make it a promising candidate to replace ductile metals in high-temperature applications.
- It's wear resistant; the extreme hardness and density of silicon carbide make it ideal for applications where parts are subject to high abrasion and sliding wear. Specified wear rate (pin on disc): SiC vs. SiC 1 x 10<sup>-9</sup> mm<sup>2</sup>/kg. Coefficient of friction (pin on disc): SiC vs. SiC 0.2.

It resists corrosion, oxidation and erosion. The high density, low porosity and chemical inertness of silicon carbide

- permit it to function in environments of hot gases and liquids, in oxidizing and corrosive atmospheres, and in strong acids and bases, even at extremely high temperatures.
- It requires minimum machining. The surface finish of silicon carbide parts is excellent (about 64 micro inches). This surface quality, combined with tight dimensional control, yields parts that should require little or no additional machining or finish grinding, depending on application.

## 2 Dynamic Models for Roller Process

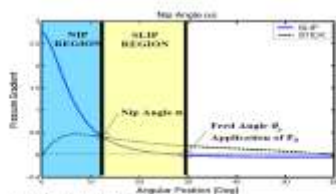


Figure 1. Determination of nip angle

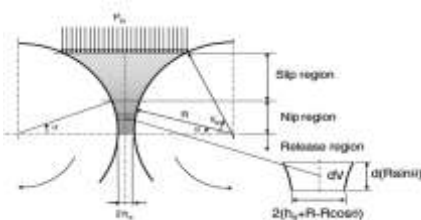


Figure 2. Johanson's Rolling Theory

The study will focus on the dynamic model of a roller compactor as described in Shuo-Huan Hsu & Gintaras V. Reklaitis 2010 using Johanson's approach. Johanson was the first to come out with a mathematical model for granulated materials. The roll press has been used widely in the still industry. Johanson provided a means to determine the press dimensions and roll forces necessary to apply the required pressure to a material with specific properties which were attained experimentally [5].

The crusher is assumed to have one fixed and one movable roll. The process parameters of the roller compactor are the speed of the roll (in rpm) and the roll pressure (in MPa). The output variables are the flake density (in g/cm<sup>3</sup>) and the gap width (in mm). Using Young's modulus and tensile strength a model can be derived.[6] It was shown by experiments [7] that the roll pressure and gap width have influence on the ribbon density at steady state, but not roll speed. On the other hand, the roll gap decreases when increasing the roll pressure and keeping other parameters constants [8]. The roll gap width is also influenced by the speeds of the feed screw and rolls. In Johanson's model the gap width is assumed to be constant which is impossible to predict the response of the gap width when the parameters are changed. [9] The material balance equation is introduced to model the characteristics of the gap width change.[10]

In Johanson's theory three areas of the material behavior in the roller compaction: slip, nip and release region were considered as shown in the figure above.

### 2.1 The Slip region:

From Jenike and Shield effective yield function:

$$\frac{d\sigma}{d\theta} = -\frac{4\sigma\left(\frac{\pi}{2}-\theta-v\right)\tan\delta}{\left(1+\frac{h_0}{R}\cos\theta\right)\left[\frac{1}{\tan(\beta-\mu)}-\frac{1}{\tan(\beta+\mu)}\right]} \quad (1)$$

where

$$\mu = \frac{\pi}{4} - \frac{\delta}{2}, v = \frac{1}{2}\left(\pi - \sin^{-1}\frac{\sin\phi}{\sin\delta} - \phi\right), \quad (2)$$

$$B = \frac{1}{2}\left(\frac{1}{2} + \phi + v\right)$$

$\delta$  is the effective angle of friction,  $\phi$  is angle of surface friction which are determined by the experiments.  $h_0$  is half of the roll gap, and  $R$  is the radius of the roll.

In the nip region, an empirical model is used to describe the compression behavior of the material given by:

$$\sigma = C_1 \rho^K \quad (3)$$

where  $\sigma$  is the material stress,  $\rho$  is the compact density,  $C_1$  and  $K$  are constants.

The nip angle is important boundary information for other models for rolling compaction of powders. It defines one of the limits for the region where most of the compaction is believed to take place. Therefore it is important to become familiar with the process and powder parameters influence on the behavior of this angle. Although it is very difficult to measure the nip angle, literature exists and states that the model provides a good estimate of the nip angle. The results are in agreement with experimental data especially for gravity fed roller presses [11].

The Nip region is given as:

$$\frac{\sigma(\theta)}{\sigma(\alpha)} = \left[ \frac{\left(1 + \frac{h_0}{R} - \cos \theta\right) \cos \alpha}{\left(1 + \frac{h_0}{R} - \cos \theta\right) \cos \theta} \right]^K \quad (4)$$

Nip angle is given as:

$$\left(\frac{d\sigma}{d\theta}\right)_{slip} = \left(\frac{d\sigma}{d\theta}\right)_{nip} \quad (5)$$

At  $\theta = \alpha$

Roll Force,  $F$  is giving as:

$$F = \frac{\sigma_{exit} R}{1 + \sin \delta} \int_0^\alpha \left[ \frac{\frac{h_0}{R}}{\left(1 + \frac{h_0}{R} - \cos \theta\right) \cos \theta} \right]^K \cos \theta d\theta \quad (6)$$

where  $\sigma_{exit} = \sigma(\theta = 0)$ .

$P_h$  is the hydraulic pressure applied on the roll and it is designed to resist this force [12]

$$F = \frac{A}{W} P_h \quad (7)$$

Rewriting equation (7)

$$P_h = \frac{A}{W} \frac{\sigma_{exit} R}{1 + \sin \delta} \int_0^\alpha \left[ \frac{\frac{h_0}{R}}{\left(1 + \frac{h_0}{R} - \cos \theta\right) \cos \theta} \right]^K \cos \theta d\theta \quad (8)$$

where  $A$  is the compact area.

From Johanson's rolling theory the following were the limitations:

- No time dependency
  - Predict steady state behaviors
  - Not suitable for control purpose
- The effects of the roll speed and speed are not considered
- The physical and mechanical properties of the material do not change

An important parameter for the initial conditions to solve equation (1) is the feed pressure.

However, in most designs today, the feed flow is driven by one or two augers. The auger aims to stabilize the feed flow. Due to the poor flowability, the auger filling may fluctuate from one revolution to another [13]. The auger provides much higher pressure than the pressure caused by the gravity, and hence the gravity effect is negligible.

Therefore, Johanson's model can be used to predict the system with not only vertically mounted rolls, but also other orientations. It is very difficult to predict the feed pressure provided by the auger [14].

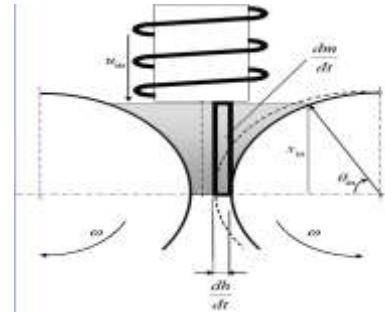


Figure 3 Johanson's mass balance model

Material Balance is given as:

$$\frac{dm}{dt} = \dot{m}_{in} - \dot{m}_{out} \quad (9)$$

$$= \rho_{in} u_{in} W (h_o + R - R \cos \theta_{in}) - \rho_{exit} R \omega \quad (10)$$

$$\Delta m = \left[ \int_0^{x_{in}} \rho dx \right] W \Delta h \quad (11)$$

$$\frac{d}{dt} \left( \frac{h_0}{R} \right) = \frac{\omega \left[ \rho_{in} \cos \theta_{in} \left( \frac{u_{in}}{\omega R} \right) \left( \frac{h_0}{R} + 1 - \cos \theta_{in} \right) - \rho_{exit} \left( \frac{h_0}{R} \right) \right]}{\int_0^{\theta_m} \rho(\theta) \cos \theta d\theta} \quad (12)$$

Equation (12) introduces the time dependency to the roller compaction model. The inlet–outlet speed ratio ( $u_{in}/\omega R$ ) directly affects the roll gap change, and the density profile  $\rho(\theta)$  needs to be solved for each time step.

In the nip region,  $\rho(\theta)$  can be easily calculated using Eq. (9), but the density–stress relationship in the slip region is not clear. Since the stress is relatively small in the slip region and does not vary in a wide range, it is further assumed that the density in this region is a constant, i.e., the same as the inlet density. With this assumption, the denominator of the right hand side of

Eq. (12) can be solved analytically:

$$\int_0^{\theta_m} \rho(\theta) \cos \theta d\theta = \rho_{exit} \left( \frac{h_0}{R} \right) \left\{ \frac{2(1+\frac{h_0}{R})}{\sqrt{\frac{h_0}{R}(2+\frac{h_0}{R})}} \tan^{-1} \left[ \sqrt{1 + \frac{2R}{h_0}} \tan \frac{\alpha}{2} \right] - \alpha \right\} + \rho_{in} (\cos v - \sin \alpha)$$

where  $\theta_{in} = \pi/2 - v$ ,  $x_{in} = R \sin \theta_{in}$ ,  $\omega$  is the angular velocity of the rolls, and  $u_{in}$  is the linear velocity of the feed, which is proportional to the rotational speed of the feed auger.

### 3. Model Representation

The transfer function of the process in the Laplace domain is given as:

$$s x(s) = A x(s) + B u(s) \quad (13)$$

$$y(s) = C x(s) + D u(s) \quad (14)$$

Eliminating  $x(s)$  the using equation (13) and inserting the expression into equation (14) gives;

$$y(s) = [C(sI - A)^{-1} B + D] u(s) \quad (15)$$

The transfer function  $H(s)$  from  $u(s)$  to  $y(s)$  :

$$H(s) = [C(sI - A)^{-1} B + D] \quad (16)$$

where

$$\frac{y}{u}(s) = H(s) \quad (17)$$

Figure 4 shows system with two inputs and two outputs:

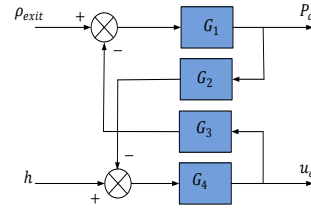


Figure 4. two input two output structure.

This will end with the transfer matrix;

$$\begin{bmatrix} \rho_{exist} \\ h \end{bmatrix} = \begin{bmatrix} \frac{G_1}{1-G_1 G_2 G_3 G_4} & -\frac{G_1 G_3 G_4}{1-G_1 G_2 G_3 G_4} \\ -\frac{G_1 G_2 G_4}{1-G_1 G_2 G_3 G_4} & \frac{G_4}{1-G_1 G_2 G_3 G_4} \end{bmatrix} \begin{bmatrix} P_d \\ u_d \end{bmatrix} \quad (18)$$

#### 3.1 Time delays

Time delays are common phenomena in many industrial processes [15]. Suppose a multivariable delayed system is defined as  $\widehat{G}_1(s)$ , in which every component is described as  $g_{ij}(s)e^{-sT_{ij}}$  for  $i = 1, 2, \dots, p1$  and  $j = 1, 2, \dots, m1$ . The structure of the delayed multivariable system is shown in Fig. 5. In order to obtain a rational transfer function, the time delay term can be approximated by a first order Padè approximation model [16,17] as,

$$e^{-sT} \approx \frac{2-sT}{2+sT} \quad (19)$$

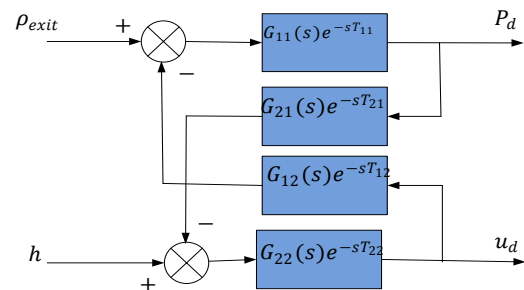


Figure 5. A delayed multivariable (2 x 2) system structure.

The state space representation with delay is given as;

$$y(s) = G(s)u(s) \quad (28)$$

where  $y(s) = [\rho_{exist}(s)h(s)]^T$ ,  $u(s) = [P_d(s)u_d(s)]^T$  and

$$\begin{bmatrix} G_{11}(s) & G_{12}(s) \\ G_{21}(s) & G_{22}(s) \end{bmatrix} = \begin{bmatrix} \frac{0.2615e^{-2.2676s}}{5.8313s + 1} & \frac{-0.0475e^{-2.2854s}}{5.8396s + 1} \\ \frac{-1.5163e^{-3.5197s}}{5.8694s + 1} & \frac{1.6863e^{-2.1068s}}{5.8097s + 1} \end{bmatrix}$$

#### 4. Instrumentation

In his paper G. Bindhumadhavan et al. / Chemical Engineering Science, 2005, proposed and experimental setup for a purpose built gravity fed roll compactor shown in (Fig.) was used. It consists of a fixed axis solid roller and a movable instrumented roller, each machined from stainless steel. The dimensions of the rollers were: diameter 20 cm and face width 4.6 cm. They were driven by stepper motors that are controlled using the LabVIEW program (National Instruments, UK). The motors were driven by a single quartz oscillator unit (McLennan Servo Supplies Ltd, UK; model PM160), which ensures a precise setting of the roller speed. An external clock was used to transmit the same impulse frequency to both motors, ensuring simultaneous rotation. The roll speed can be varied from 0.5 to 20 rpm. In order to prevent leakage of the material, the sides of the rolls were sealed using cheek plates. The instrumented roller is fitted with a miniature piezo-electric transducer (PCB Piezotronics Inc, USA; model 105C33) in order to measure the pressure profile normal to the roll surface; it was specified for a maximum pressure of 120MPa. This involved the use of a specially segmented roller for accommodating the transducer. The signals from the transducer were transmitted by means of a slip ring assembly to a computer via an analog/digital converter card (National Instruments, UK; model SCB 68). The gap between the rolls can be varied from 0 to 5 mm, which was measured by using two LVDT displacement transducers (Solatron Metrology, UK; model DFg5). An absolute encoder that was mechanically coupled to the instrumented roller shaft was employed to measure the angular position of the pressure transducer simultaneously with the

pressure measurement. A rectangular hopper was used to feed the powder into the rollers. [20]

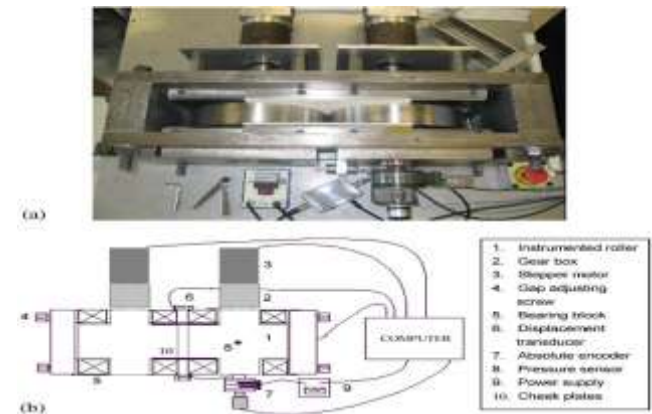


Figure 6. Instrumented Roller Crusher

Measure of roll gap, the roll gap can be made by collecting the signal from a pair of gap sensor installed at both sides of monitor frame which serves as the reference plane of measuring sensor with calibrated thickness. By using sampling rate considered gap sensor design and high speed data processing scheme, measuring accuracy is ensured regardless of variable dummy bar traveling speed.

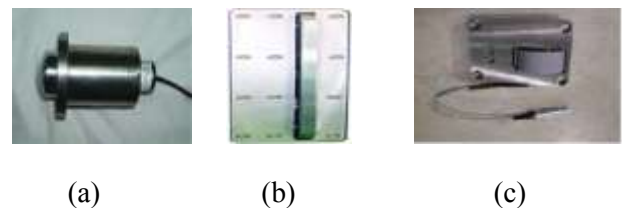


Figure 7. a) Roll Gap Sensor; b) Roll Alignment, c) Roll Speed.

Measure of roll bending /wearing: the bending of the rolls can be done in two ways; (1) by measuring the distance to outer roll surface at different locations across the width direction (2) by measuring roll gap at multiple points through circumference of circular roll and comparing the deviation between the measured values

Measurement of roll alignment, this is made only for fixed side roll arrangement showing the magnitude of roll misplacement. By double checking of misaligned angle of the target roll against fore and rear side placed rolls, the shortcomings of sequential measurement of relative angle can be recovered.

Measurement of roll rotation; this is determined as the slip ratio of wheel of rotation sensor which

contact with the surface of the caster roll. If the roll bearing condition is so good as to rotate freely by dragging force of the anvil friction, there happens no slip between sensing wheel and roll as to generate no signal to rotation sensor [21].

#### 4.1 Mass flow control

For a 2 Kg/h (capacity): there are 3 different sensors for measuring the kg/h ratio: one in the milling loop (after the HTV), one in the overflow pipeline (slissa) and the last one measuring the amount of material going through the classifier (600/f). In principle, they all work as volume based (differently from previous systems, where it was weight based). The volume based measures the time needed to fill a certain volume (level sensor). According to this time and assuming a certain specific density, the system is able to calculate the amount of material per time [22].

In instrumented compaction roller sensors, each sensor is instrumented for two channels of analog output corresponding to normal and shear stress. Normal stress is proportional to sum of output from two sensors and shear stress is proportional to difference of output from two sensors [23]. A temperature sensor is installed to measure the temperature of crushed material. 4-20ma [24].

Uses of instrumented roll are listed in the following:

- Changing roller compaction process parameters impacts the degree of densification
- The stress profile in the powder determines the density of the resulting compact
- In general, material density can be predicted from the normal stress using the relationship given below;

$$\rho^K \propto \max\{\sigma_N\} \propto \int_A \sigma_N(\theta, z) dA = F_{roll} \propto \text{roll pressure} \tag{29}$$

where  $F_{roll}$  total roll force (kN);  $\sigma_N$  normal (compressive) stress (MPa);  $\rho$  material apparent density (g/cm<sup>3</sup>); A area of sensor surface (mm<sup>2</sup>); K

compressibility of powder;  $\theta$  roll angle of rotation (°); z position across roll width (mm).

### 5. Simulation Results

Padé approximations are used to approximate the delay terms. With the use of Simulink, the accurate model can be established as shown in Figure 6. When the Simulink model is established, the following statements can be used in the linearization process, and one can obtain the linear state space model. The exact simulation results are obtained, together with the linearized model, as shown in Figure. It can be seen that the simulation results of the linearized model are very accurate [18].

$$\begin{aligned} \dot{x} &= \begin{bmatrix} -1.054 & -0.3026 & 0 & 0 & 0 & 0 & 0 & 0 \\ 0.5 & 0 & 0 & 0 & 0 & 0 & 0 & 0 \\ 0 & 0 & -0.7386 & -0.3872 & 0 & 0 & 0 & 0 \\ 0 & 0 & 0.25 & 0 & 0 & 0 & 0 & 0 \\ 0 & 0 & 0 & 0 & -0.8719 & -0.48 & 0 & 0 \\ 0 & 0 & 0 & 0 & 0.25 & 0 & 0 & 0 \\ 0 & 0 & 0 & 0 & 0 & 0 & -1.121 & -0.3268 \\ 0 & 0 & 0 & 0 & 0 & 0 & 0.5 & 0 \end{bmatrix} \\ &+ \begin{bmatrix} 0.25 & 0 \\ 0 & 0 \\ 1 & 0 \\ 0 & 0 \\ 0 & 0.125 \\ 0 & 0 \\ 0 & 1 \\ 0 & 0 \end{bmatrix} u \\ y &= \begin{bmatrix} -0.1485 & 0.262 & 0 & 0 & 0.06507 & -0.1824 & 0 & 0 \\ 0 & 0 & 0.2583 & -0.5872 & 0 & 0 & -0.2903 & 0.5511 \end{bmatrix} \end{aligned} \tag{30}$$

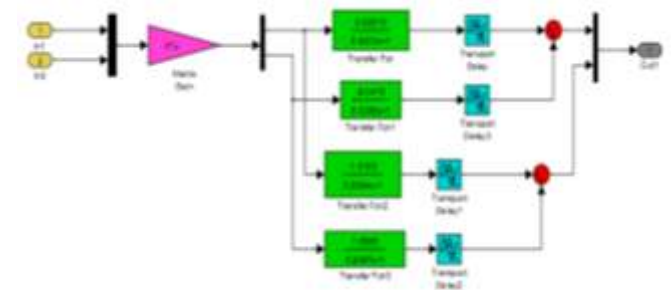


Figure 8. Simulink diagram with delay

TABLE I. SYSTEM PARAMETERS

Variables	Description	Values
$\delta$	Effective angle of friction	$40.5^\circ$
$\theta$	Angle of wall friction	$18.0^\circ$
R	Radius of the rollers	12.5cm
A	Compact surface area	$100\text{cm}^2$
W	Roll width	5cm
$\tau_p$	Time constant of the roll force response due to the change of hydraulic pressure	6s
$\tau_\omega$	Time constant of the roll speed response	6s
$\tau_u$	Time constant of the feed speed response	6s
$\rho_{in}$	Inlet density	$0.3\text{ g/cm}^3$
C1	Pre-exponential coefficient in the model of material compression	$7.5 \times 10^{-8}\text{ Pa}(\text{kg/m}^3)^{4.97}$
K	Compressibility factor	4.97
$2h_0$	roll gap width	3.66 mm
$\rho_{exist}$	Compact density at exit point	$0.900\text{ g/cm}^3$
Pd	Hydraulic pressure (set point)	1 MPa
$\omega_d$	Angular velocity of the rolls	5 rpm
ud	Feed speed	3.27 cm/s

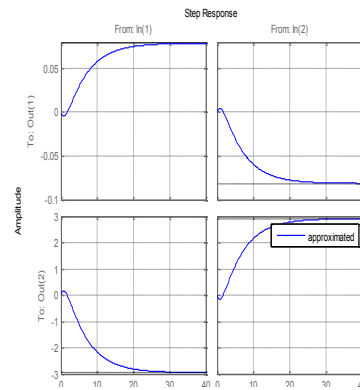
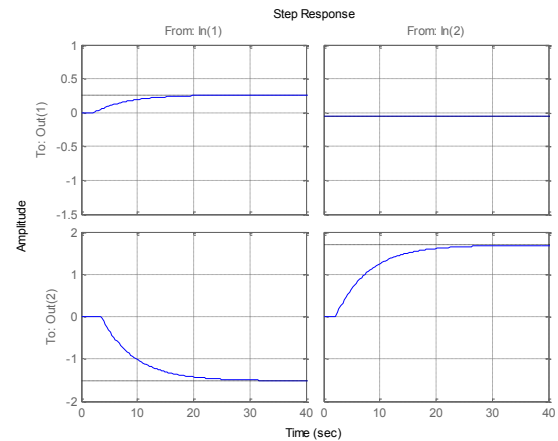


Figure 9 A step response for uncompensated system with Padé approximation



Step response without an approximation

## 6 Conclusion

The paper presented the use of Johansen model in modelling the roller crusher was achievable using Matlab. This paper also identified areas of the roller crusher where sensors are placed. As a future work, a Model Predictive Control design for the process is under investigation.

### References:

- [1]Grimble, M.J., Robust Industrial Control: Optimal Design Approach for Polynomial Systems, Prentice Hall, 1994, p. 261 and pp. 443-456
- [2]Weir Minerals |KHD Humboldt Wedag 2010
- [3]Topalov, A. V., Kaynak, O., 2004. "Neural network modeling and control of cement mills using a variable structure systems theory based

- on-line learning mechanism”, *Journal of Process Control*, Vol. 14, p. 581.
- [4] M.J. Daniel, S. Morrell (2004), ‘HPGR model verification and scale-up’, Julius Kruttschnitt Mineral Research Centre, The University of Queensland, Isles Road, Indooroopilly, Qld. 4068, Australia
- [5] Shuo-Huan Hsu & Gintaras V. Reklaitis & Venkat Venkatasubramanian Modeling and Control of Roller Compaction for Pharmaceutical Manufacturing. Part I: Process Dynamics and Control Framework 18 March 2010.
- [6] R. Johnson, (1965) “A rolling theory for granular solids,” *ASME, Journal of Applied Mechanics* 32 : series E. No. 4,
- [7] Marshall EA. A theory for the compaction of incompressible granular materials by rolling. *J Inst Math Appl.* 1973;12(1):21–36
- [8] J.R. Johnson, (1965) “A rolling theory for granular solids,” *ASME, Journal of Applied Mechanics* 32 : series E. No. 4,
- [9] Jenike A.W, Shield RT. On the plastic flow of Coulomb Solids beyond original failure. *Trans ASME: J Appl Mech B.* 1959;81:599–602.
- [10] JenikeAW, Shield RT. On the plastic flow of Coulomb Solids beyond original failure. *Trans ASME: J Apply Mech B.* 1959;81:599–602 *Apply Mech B.* 1965;32(4):842–8.
- [11] Marshall EA. A theory for the compaction of incompressible granular materials by rolling. *J Inst Math Appl.* 1973;12(1):21–36.
- [12] Shuo-Huan Hsu & Gintaras V. Reklaitis & Venkat Venkatasubramanian Modeling and Control of Roller Compaction for Pharmaceutical Manufacturing. Part I: Process Dynamics and Control Framework 18 March 2010
- [13] Shlieout G, Lammens RF, Kleinebudde P. Dry granulation with a roller compactor. Part I: the functional units and operation modes. *Pharma Tech Europe.* 2000;12(11):24–3
- [14] Panelli R, Ambrozio F. Compaction equation and its use to describe powder consolidation behaviour. *Powder Metall.* 1998;41 (2):131–3.
- [15] Zhang, W.D., and X.M. Xu, “Optimal Solution, Quantitative Performance Estimation, and Robust Tuning of the Simplifying Controller,” *ISA Trans.*, Vol. 41, No. 1, pp. 31-36 (2002)
- [16] Goodwin, G.C., S.F. Graebe, and M.E. Salgado, *Control System Design*, Prentice Hall, NJ, U.S.A., pp. 267-268 (2001)
- [17] Wang, Q.G., C.C. Hang, and X.P. Yang, “Single-Loop Controller Design via IMC Principles,” *Automatica*, Vol. 37, No. 12, pp. 2041-2048 (2001)
- [18] Dingyü Xue, YangQuan Chen, Derek P. Atherton (2007). “Linear Feedback Control Analysis and Design with MATLAB” Society for Industrial and Applied Mathematics Philadelphia PP. 131,135